PHYSICAL REVIEW A **91**, 051805(R) (2015)

Attonewton force detection using microspheres in a dual-beam optical trap in high vacuum

Gambhir Ranjit, David P. Atherton, Jordan H. Stutz, Mark Cunningham, and Andrew A. Geraci*
Department of Physics, University of Nevada, Reno 89557, Reno Nevada, USA
(Received 3 April 2015; published 26 May 2015)

We describe the implementation of laser-cooled silica microspheres as force sensors in a dual-beam optical dipole trap in high vacuum. Using this system we have demonstrated trap lifetimes exceeding several days, attonewton force detection capability, and wide tunability in trapping and cooling parameters. Measurements have been performed with charged and neutral beads to calibrate the sensitivity of the detector. This work establishes the suitability of dual-beam optical dipole traps for precision force measurement in high vacuum with long averaging times, and enables future applications including the study of gravitational inverse square law violations at short range, Casimir forces, acceleration sensing, and quantum optomechanics.

DOI: 10.1103/PhysRevA.91.051805 PACS number(s): 42.50.Wk, 07.10.Cm, 07.10.Pz

I. INTRODUCTION

Micro- and nanomechanical oscillators have achieved attonewton force sensitivity, enabling the detection of single-electron spins in solids [1], tests for non-Newtonian gravity at submillimeter length scales [2], and the realization of sensitive chip-scale optomechanical force transducers [3–5] and accelerometers [6]. Nanotube resonators have recently demonstrated sensitivity well below the aN/$\sqrt{\text{Hz}}$ level in a cryogenic system [7].

The minimum detectable force in the presence of thermal noise scales with the inverse square root of the mechanical quality factor Q, which is typically limited by materials loss including thermoelastic dissipation and surface imperfections, as well as clamping loss. To circumvent clamping loss, one can consider levitating the mechanical oscillator, for example using magnetic fields [8] or radiation pressure [9]. For a sufficiently rigid particle in such a trap, its center-of-mass oscillations are largely unaffected by the internal loss mechanisms in the material, while still being damped by collisions with the background gas. Thus by optical trapping in a high vacuum environment, excellent decoupling is achieved, leading to subattonewton sensitivity even in a room temperature environment [9]. Such sensitivity enables new searches for gravitational inverse square law violations at short range [10], tests of Casimir forces in new regimes [10], new methods for the detection of gravitational waves [11], as well as sensitive electromagnetic and inertial sensing [9].

Levitated dielectric objects have also been identified as promising candidates for ground state cooling [12,13], tests of quantum phenomena in mesoscale systems [12–14], precision interferometry [15,16], and hybrid quantum systems coupled to cold atoms [17]. While the first optical trapping and manipulation of microscopic dielectric particles in vacuum was reported in the 1970s by Ashkin and co-workers [18–20], several recent experiments have revitalized this field, involving millikelvin feedback cooling of dielectric spheres in a dual-beam optical trap [21], parametric feedback cooling of nanospheres in an optical tweezer in high vacuum [22], cavity cooling of a nanosphere in an optical cavity trap [23], searches for millicharged particles in an optical levitation trap [24], and trapping and cavity cooling of a nanoparticle in a combined optical and ion trap in high vacuum [25].

In this Rapid Communication, we report the use of laser-cooled silica microspheres as force sensors in a dual-beam optical dipole trap in high vacuum. A significant challenge in the realization of optically trapped dielectric particles at low pressure has to do with the ability to stabilize the particle while pumping through the regime of intermediate vacuum [20,23]. We have identified a set of trapping and laser-cooling conditions that provide a robust method to pump beads through this transition region between diffusive and ballistic collisions with the surrounding gas molecules. Previous work in a dual-beam dipole trap had achieved high-vacuum lifetimes of order ∼1 h [21]. Here we have regularly attained trap lifetimes of several days, limited only by applied perturbations which resulted in loss of the particle. In contrast to Ashkin-type single beam levitation traps [20,24] where the scattering force from a vertically oriented laser beam balances the gravitational acceleration g due to the Earth, the dual-beam trap affords a wider tunability of trap parameters. For example, the position of the trapped particle can be made less dependent on the trapping laser intensity.

The force fluctuation spectral density due to thermal noise for a harmonic oscillator at temperature T is

$$S_{\text{F}}^{1/2} = \sqrt{\frac{4k_B T k}{\omega_0 Q}}, \tag{1}$$

where k is the spring constant and w_0 is the resonance frequency. The minimum resolvable force in a measurement of bandwidth b is thus $F_{\text{min}} = \sqrt{\frac{4k_B T k b}{\omega_0 Q}}$. For a microsphere of mass m in the absence of laser cooling, $F_{\text{min}} = \sqrt{4k_B T m \Gamma_M b}$, where $\Gamma_M = 16P/(\pi\rho v r)$ is the damping rate of a sphere with radius r and density ρ due to background gas with pressure P and mean speed v. For a sphere cooled with laser feedback cooling, the temperature in Eq. (1) becomes T_{eff} and the damping rate Γ_{eff} includes the effect of the cooling laser. Using this system we have demonstrated $S_{\text{F}}^{1/2}$ of order 200 aN/$\sqrt{\text{Hz}}$, with a corresponding acceleration sensitivity of ∼700 μg /$\sqrt{\text{Hz}}$ using a 30 pg test mass. The force sensitivity is comparable to that achieved with cryogenic Microelectromechanical systems resonators used in Ref. [2], and approaching the sensitivity of current state-of-the-art room temperature optomechanical

*ageraci@unr.edu

force sensors [3–5] within a factor of ∼3. We estimate that with improved laser noise, subattonewton/$\sqrt{\text{Hz}}$ sensitivity and performance competitive with nanogram optomechanical accelerometers [6] (∼10 μg /$\sqrt{\text{Hz}}$) may be achievable. Time-averaged measurements with attonewton sensitivity have been performed. Measurements with known electric fields applied to charged and neutral beads have been performed to calibrate the detection method. This work establishes the feasibility of versatile, robust, dual-beam optical dipole traps for precision force measurement in high vacuum with long averaging times, enabling the studies of gravitational inverse square law violations at short range, Casimir forces, acceleration sensing, and quantum optomechanics.

II. EXPERIMENTAL SETUP

The experimental setup is illustrated in Fig. 1. A 3 μm fused silica sphere is trapped within an optical dipole trap created by focusing two 1064 nm counterpropagating orthogonally polarized beams of roughly equal power to the nearly same position in space. The initial total power is 2.2 W and the waist size is approximately 8 μm. The beam foci are offset axially by 75 μm to allow for greater power imbalance between the beams. The foci offset is adjusted by moving the dipole trap lenses which are mounted on in-vacuum translation stages. The offset is measured *ex situ* using a pinhole mounted on a three-dimensional (3D) translation stage. Figure 2 shows the optical scattering and gradient force on a bead along the axial direction, as calculated with Lorenz-Mie theory [26]. For zero foci offset, the power balance must be maintained below the 1% level to obtain a stable trap. For larger focal separation this requirement is greatly relaxed. A piezoelectric

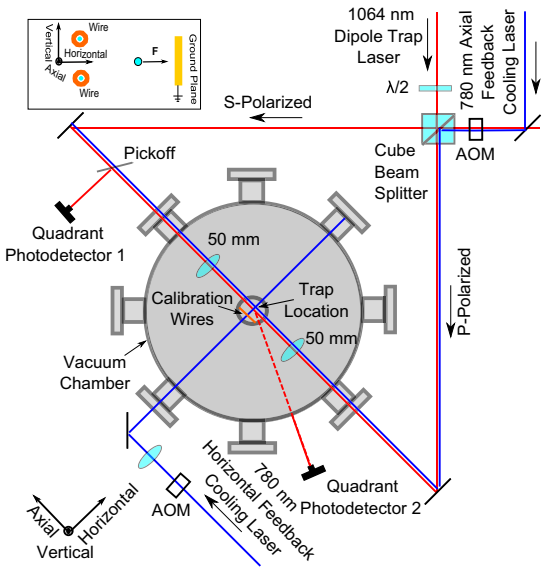

FIG. 1. (Color online) The optical dipole trap is created by focusing two orthogonally polarized laser beams using 50 mm focal length inside a vacuum chamber. A 780 nm laser provides active feedback cooling to stabilize the trapped beads in vacuum and provide optical damping. Inset: A set of calibration electrodes is used to conduct force measurements with a known applied electric field at the location of the trap.

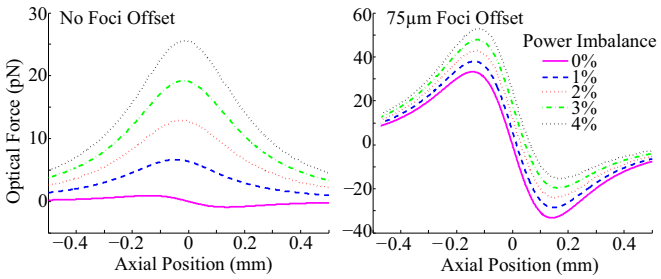

FIG. 2. (Color online) Optical force along the laser axis with coincident foci (left) and offset foci (right) for various power imbalance between the *S*- and *P*-polarized beams. Power imbalance is defined so that, e.g., 1% indicates 51% of the power is in the *P*-polarized beam. The total laser power is 2.2 W and the waist is 9 μm.

transducer (PZT) driven mirror allows *in situ* adjustment of the transverse alignment of the beams. To load the trap, an in-vacuum PZT is used to vibrate a glass substrate above the trap center which has beads deposited on it. The trap is typically loaded at 5–10 Torr of N_2 gas.

The 3D position of the microsphere is measured using two separate quadrant photodetectors (QPDs). For active feedback stabilization, the position signals from the QPDs are phase shifted by 90° to provide a signal proportional to the bead's instantaneous velocity using either a derivative circuit or phase shifter circuit. The phase shifted signals were used to modulate the rf amplitude of three acousto-optic modulators, which modulate the intensity of a 780 nm laser, providing a velocity-dependent damping force in each direction. The feedback light is focused onto the sphere using 200 mm lenses outside of the vacuum chamber in the vertical (y) and horizontal (x) directions, and using one of the dipole trap lenses for the axial (z) direction.

Without feedback cooling, particles are lost from the trap as the pressure is pumped from approximately 1 Torr to high vacuum. Figure 3(a) shows the pressure at which microspheres are lost from the trap, as a function of laser intensity. There is a marked increase in the pressure at which beads are lost for laser intensity exceeding approximately 4×10^9 W/m^2, whereas the pressure remains relatively constant below this point. Assuming a conservative trap, the trapping depth determined by the dipole potential is given by $U = \frac{3I_{\text{trap}}V}{c}\frac{\epsilon_1-1}{\epsilon_1+2}$, where V is the volume of the microsphere and ϵ_1 is the real part of the relative permittivity. For our parameters for a 3 μm sphere the trap depth is approximately 2.5×10^6 K ($\frac{I_{\text{trap}}}{10^9\ \text{W/m}^2}$). Although this trapping depth increases linearly with intensity, the particle loss effect may have to do with instabilities due to nonconservative scattering forces in the optical trap [27,28] which are enhanced at higher laser power. We have observed that for poor trapping alignment, these nonconservative forces are able to drive cyclic motion in the trap and under these conditions the particle is subject to loss even at pressures exceeding 1 Torr for similar trapping intensities. By steering the trapping beam overlap using PZT mirrors, these effects can be reduced.

The particle loss in Fig. 3(a) also may have to do with radiometric forces [20,29]. The finite optical absorption in the sphere results in an increased surface temperature. As gas molecules collide with the surface, they carry away larger

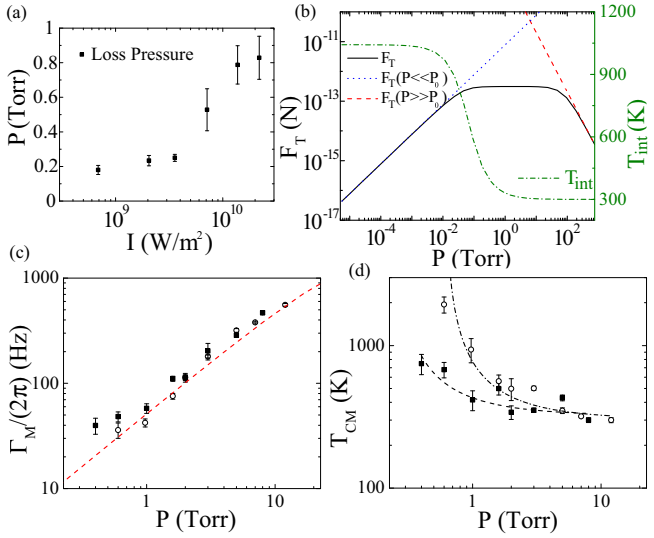

FIG. 3. (Color online) (a) Mean pressure at which beads are lost from the trap for various laser trapping intensities, with no laser-feedback cooling applied. Statistics are shown for 30 beads. (b) Calculated internal temperature (right) and photothermal force (left) assuming $\epsilon_2 = 10^{-6}$ and 1% internal temperature gradient across the bead. (c) Measured damping rate along x versus gas pressure for two different beads (dashed line). Calculated damping rate for a bead of diameter 3.0 μm in N_2 gas. (d) Measured center-of-mass temperature in the x direction versus pressure. For data shown in (b)–(d), $I_{\text{trap}} = 2 \times 10^9$ W/m^2.

kinetic energy. Currents of these hot air molecules produced by gradients in the trapping intensity can, in principle, cause the particles to be kicked from the trap [20]. We can parametrize the optical absorption through the imaginary part of the complex permittivity $\epsilon = \epsilon_1 + i\epsilon_2$. Bulk silica has approximately $\epsilon_2 = 10^{-7}$ [30]. We can place an upper bound on $\epsilon_2 < 10^{-6}$ by observing that the trapped sphere does not evaporate under high vacuum conditions at high laser intensity. We expect ϵ_2 is within this range. In Fig. 3(b) we show the expected mean internal temperature T_{int} of the bead for $\epsilon_2 = 10^{-6}$ as a function of gas pressure. In this model, at high pressure the sphere is cooled through gas collisions, while at high vacuum conditions the heat is dissipated through blackbody radiation. A lower ϵ_2 results in a lower high-vacuum equilibrium temperature, however the shape of the curve is qualitatively similar. T_{int} begins to appreciably rise at pressures around 1 Torr.

Figure 3(b) also shows the expected dependence of the photothermal force on pressure, following the model of Ref. [31], where we take into account that the temperature gradient depends on the pressure. There is a region between ~100 mTorr and 10 Torr where the magnitude of the photothermal force F_T is independent of pressure. This result is in contrast to the early work shown in Ref. [20] where a fixed temperature gradient was assumed, resulting in a local maximum at $P = P_0$, where $P_0 = \frac{3\eta}{r}\sqrt{\frac{R_g T_{\text{gas}}}{M}}$. Here η, T_{gas}, and M are the N_2 viscosity, temperature, and molar mass, respectively, and $R_g = 8.31 \frac{\text{J}}{\text{mol K}}$ is the gas constant. In the flat region the temperature gradient is increasing as $1/P$ while the photothermal force is proportional to P. At sufficiently low pressure (e.g., below 10^{-2} Torr) the temperature is set by blackbody radiation and the temperature gradient becomes constant. To estimate the magnitude of F_T we assume a 1% variation in temperature across the 3 μm sphere, due to the intensity gradient of the trapping beams near their waists. The shape of this curve is qualitatively similar for larger or smaller temperature variations within an order of magnitude. Thus there is generally a range of intermediate vacuum pressures over which photothermal forces can be significant.

Taking into account the heating rate due to nonconservative forces from the scattering force, from radiometric forces, and from laser noise, we estimate the steady state average phonon number in the trap (considering only one dimension for simplicity): $\bar{n} = (\bar{n}_{\text{th}}\Gamma_M + \Gamma_{\text{sc}})/(\Gamma_M + \Gamma_{\text{cool}} - \alpha_{\text{NC}})$. Here Γ_M is the damping rate due to the background gas, Γ_{cool} is the laser cooling rate, and $\bar{n}_{\text{th}}\Gamma_M$ is the thermalization rate due to the environmental heat bath of the surrounding gas. The term Γ_{sc} includes heating from laser noise and momentum diffusion due to photon recoil, while the term α_{NC} corresponds to heating due to nonconservative forces from the scattering force and the radiometric force: $\alpha_{\text{NC}} \equiv \alpha_{\text{NC(rad)}} + \alpha_{\text{NC(trap)}}$. In Fig. 3(c) we show the measured damping rate for motion in the x direction for two different beads, with no laser cooling applied. There is reasonable agreement with the calculated damping rate from N_2 gas [32], shown as a dashed line for a sphere with a diameter of 3 μm, within experimental uncertainties. Figure 3(d) shows the corresponding center-of-mass temperature of the beads motion in the x direction as a function of pressure. With laser cooling turned off, i.e., $\Gamma_{\text{cool}} = 0$, we can estimate the value of α_{NC} from the pressure at which the beads are lost, corresponding to the vanishing of the denominator in the expression for $\bar{n}$. At this point the damping rate from the gas is approximately equal to the heating rate from the radiometric forces and nonconservative scattering forces. The experimentally inferred heating rate α_{NC} typically ranges from 20 to 50 Hz. Variance in this value may depend on the absorption coefficient of a particular bead, or on the trap alignment. Other groups have reported loss pressures in the mTorr range in the absence of feedback cooling [21,22]. These differences might also have to do with reduced optical absorption or improved trap alignment. For example, the tweezer used in Ref. [22] has no beam overlap issues.

To avoid the trapping instabilities, we reduce the laser trap intensity I_{trap} to approximately 2×10^9 W/m^2 prior to pumping to high vacuum. In this case laser feedback cooling is able to provide damping needed to stabilize the particle as it is pumped to high vacuum using a turbomolecular pump. The intensity of the feedback light is typically ~10^7 to 10^8 W/m^2, in the x, y, and z directions. The feedback gain is increased until the linewidth of the mechanical resonance is roughly ~400 to 500 Hz in the transverse directions and ~300 Hz in the axial direction. The N_2 is slowly removed from the chamber by slowly opening a right angle valve over several minutes, until the pressure is below 10^{-4} Torr. At this point the valve can be opened completely and the base pressure of the chamber of approximately 5×10^{-6} Torr is reached. After high vacuum has been attained, the laser cooling rate can be reduced by more than an order of magnitude, while still allowing the particle to remain trapped for long time periods. It is also possible to turn off the feedback in one direction and still maintain the particle in the trap, due to cross-coupling between feedback

channels. This is suggestive that radiometric forces present at intermediate pressures, not solely the nonconservative scattering forces, play a role in the trap loss mechanism. I_{trap} can be increased by a factor of ∼5 at high vacuum before losing the particle. This allows the trapping frequency to be tuned by more than a factor of 2 *in situ*. The loss at high vacuum with high intensity may be due to nonconservative forces in the trap or internal heating.

Prior to pumping to high vacuum, the temperature as derived from the position spectrum of the beads is largely independent of pressure for sufficiently high pressure, as shown in Fig. 3(d). We thus assume the bead is in thermal equilibrium with the background gas above 5 Torr. This allows us to determine a scale factor to convert the quadrant photodetector voltage into a displacement.

Figure 4(a) shows a typical 3D position spectrum of a bead held at low vacuum of 1.7 Torr with no feedback cooling applied, and a spectrum at high vacuum of 5×10^{-6} Torr with feedback cooling. The transverse modes (x,y) are observed with frequencies of 1073 and 1081 Hz, respectively, and the axial (z) frequency is 312 Hz. The peaks are slightly shifted when feedback cooling is applied due to the optical spring effect that occurs if the feedback phase is not precisely 90°. Under high vacuum conditions with feedback cooling applied, using a Lorentzian fit we attain effective temperatures of 10 ± 3 K, 55 ± 9 K, and 12 ± 2 K in the x, y, and z directions, respectively, with corresponding damping rates of 454 ± 29 Hz, 448 ± 16 Hz, and 340 ± 120 Hz. The force sensitivity in the x direction corresponds to $S_{F,x}^{1/2} = 217 \pm 48$ aN/$\sqrt{\mathrm{Hz}}$, with the error dominated by the uncertainties in the particle size and the displacement-to-voltage scaling factor for the quadrant photodetector. The lowest attainable temperature appears to be limited by noise in the trapping laser. The expected sensitivity at this pressure would be approximately 10^2 times lower in the absence of laser noise and cross-talk between feedback channels. Figure 4(b) shows the x spectrum of a bead at 5×10^{-6} Torr with varying feedback cooling rates. The beads remain trapped at high vacuum using feedback damping rates less than 10% of the values needed while evacuating the chamber.

III. FORCE MEASUREMENTS

In the absence of an applied force, we expect the signal due to thermal noise to average down as $b^{1/2}$. This behavior is shown in Fig. 5(a) for averaging times exceeding 10 h. Force sensitivity of ∼2 aN is achievable at this time scale. Figure 1 depicts the wire configuration used to produce a known electric field E_x at the position of the bead. We apply a sinusoidal voltage ranging from $V_{\mathrm{ac}} \sim 2$–28 V to the two wires, corresponding to electric fields up to 2300 V/m. We find that approximately 80% of beads are trapped with a nonzero charge. Those beads which are neutral after trapping remain neutral over the time scale of our measurements, which we have extended over several days. The beads which are charged tend to retain the same value of charge. By implementing suitable UV light source, control of the bead charge should be possible [24]. In earlier work at low vacuum (1.7 Torr), we have found that by applying UV light in the vacuum chamber the bead charge can be reduced *in situ* [33].

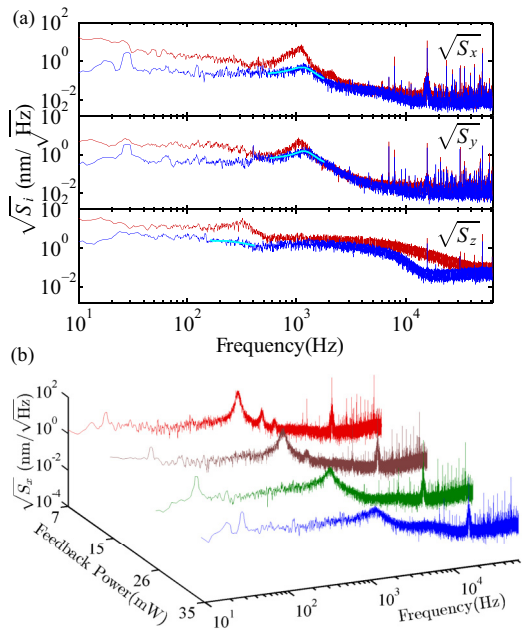

FIG. 4. (Color online) (a) Typical position spectrum of a bead held at low vacuum of 1.7 Torr with no feedback cooling applied (red), and at high vacuum of 5×10^{-6} Torr with feedback cooling applied (blue). Also shown (light blue) is a Lorentzian fit to the peaks in the high vacuum data, with fit parameters as discussed in the text. (b) x spectrum of a bead at 5×10^{-6} Torr with varying feedback cooling rates.

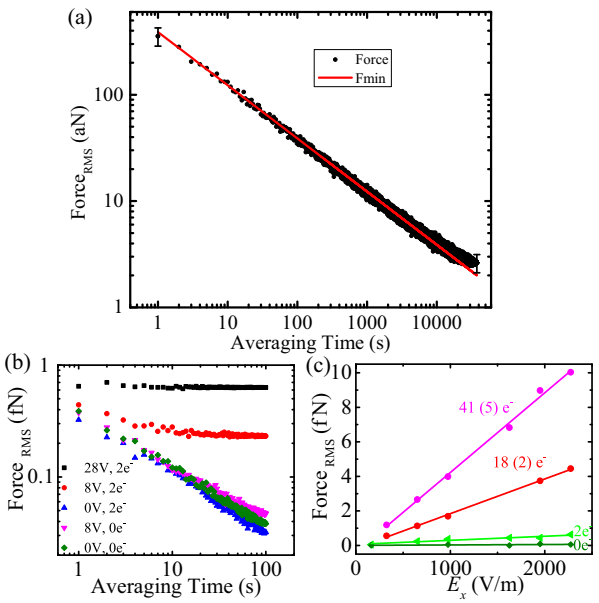

FIG. 5. (Color online) (a) On-resonance horizontal (x) force on the bead at 5×10^{-6} Torr, versus averaging time, with no applied forces. (b) Force on a charged bead ($2e^-$) and neutral bead ($0e^-$) versus averaging time for varying applied driving voltage V_{ac}. (c) Force on beads of varying charge (neutral, $2e^-$, $18 \pm 2e^-$, and $41 \pm 5e^-$) versus applied driving voltage V_{ac} and corresponding electric field with 100 s averaging time. Data are shown at $V_{\mathrm{ac}} =$ 2,4,8,12,20,24,28 V.

In Fig. 5(b) we show the force on a charged bead and neutral bead as a function of averaging time, for different values of applied electric field. When the applied field is turned off, the noise floor averages down as expected. These measurements are performed near the trap resonance frequency ≈ 1.1 kHz. Measurements are also taken off resonance at 7 kHz, where the mechanical response of the bead is significantly reduced, and without a bead in the trap to determine the electronic background noise. We find the electronic noise is not significant over the 100 s time scale for driving voltages V_{ac} up to 8 V. From the known E_x and the observed displacement of the bead, the measured value of the charge is 1.83 ± 0.21 electrons, so we assign the value $2e^-$. In Fig. 5(c) we show the force versus applied electric field for several different beads with differing charges. The sign of the charge is determined by measuring the phase of the motion with respect to the applied voltage. Measurements with beads having a known small number of electrons (e.g., one or two) provide an independent calibration of the force sensitivity.

IV. DISCUSSION

We have determined a set of trapping and cooling parameters which permit pumping through the intermediate vacuum transition where trap instabilities are known to be present. At high vacuum we have demonstrated force sensitivity at the attonewton level, with trapping lifetimes exceeding days. We estimate that improved sensitivity of order 10^2 can be attained with reduced laser noise at similar pressures, for example by using an intensity-stabilized laser in a standing wave trap to reduce the effect of beam pointing fluctuations in the counterpropagating beams. Also, nonconservative heating effects due to the scattering force should be reduced in such a trap, due to improved overlap of the counterpropagating lasers. Our method produces trapped beads with zero or negative charge, which remains constant over the trap lifetime at high vacuum. This system shows promise for precision measurements in ultrahigh vacuum requiring long averaging times, including tests of short-range gravitational forces or Casimir forces, as well as experiments on quantum optomechanics, for example where silica beads are held in a dual-beam dipole trap and cooled using a cavity [13], with feedback cooling [34], or by sympathetic cooling with atoms [17].

ACKNOWLEDGMENTS

We are grateful to Melanie Beck, Chris Thomas, and Darren Zuro for experimental assistance at the early stages of this work. We thank T. Li, J. Weinstein, M. Aspelmeyer, and N. Kiesel for useful discussions. This work is supported by Grant No. NSF-PHY 1205994.

[1] D. Rugar, R. Budakian, H. J. Mamin, and B. W. Chui, Nature (London) **430**, 329 (2004).
[2] A. A. Geraci, S. J. Smullin, D. M. Weld, J. Chiaverini, and A. Kapitulnik, Phys. Rev. D **78**, 022002 (2008).
[3] H. Miao, K. Srinivasan, and V. Aksyuk, New J. Phys. **14**, 075015 (2012).
[4] E. Gavartin, P. Verlot, and T. J. Kippenberg, Nat. Nanotechnol. **7**, 509 (2012).
[5] C. Doolin, P. H. Kim, B. D. Hauer, A. J. R. MacDonald, and J. P. Davis, New J. Phys. **16**, 035001 (2014).
[6] A. G. Krause, M. Winger, T. D. Blasius, Q. Lin, and O. Painter, Nat. Photonics **6**, 768 (2012).
[7] J. Moser, J. Guttinger, A. Eichler, M. J. Esplandiu, D. E. Liu, M. I. Dykman, and A. Bachtold, Nat. Nanotechnol. **8**, 493 (2013).
[8] P. Eizinger, W. Schoepe, K. Gloos, J. T. Simola, and J. T. Tuoriniemi, Physica B **178**, 340 (1992); O. Romero-Isart, L. Clemente, C. Navau, A. Sanchez, and J. I. Cirac, Phys. Rev. Lett. **109**, 147205 (2012).
[9] Z. Q. Yin, A. A. Geraci, and T. Li, Int. J. Mod. Phys. B **27**, 1330018 (2013).
[10] A. A. Geraci, S. B. Papp, and J. Kitching, Phys. Rev. Lett. **105**, 101101 (2010).
[11] A. Arvanitaki and A. A. Geraci, Phys. Rev. Lett. **110**, 071105 (2013).
[12] D. E. Chang, C. A. Regal, S. B. Papp, D. J. Wilson, J. Ye, O. Painter, H. J. Kimble, and P. Zoller, Proc. Natl. Acad. Sci. USA **107**, 1005 (2010).
[13] O. Romero-Isart, M. L. Juan, R. Quidant, and J. Ignacio Cirac, New J. Phys. **12**, 033015 (2010).
[14] O. Romero-Isart, Phys. Rev. A **84**, 052121 (2011).
[15] J. Bateman, S. Nimmrichter, K. Hornberger, and H. Ulbricht, Nat. Commun. **5**, 4788 (2014).
[16] A. A. Geraci and H. Goldman, arXiv:1412.4482.
[17] G. Ranjit, C. Montoya, and A. A. Geraci, Phys. Rev. A **91**, 013416 (2015).
[18] A. Ashkin, Phys. Rev. Lett. **24**, 156 (1970).
[19] A. Ashkin and J. M. Dziedzic, Appl. Phys. Lett. **19**, 283 (1971).
[20] A. Ashkin and J. M. Dziedzic, Appl. Phys. Lett. **28**, 333 (1976).
[21] T. Li, S. Kheifets, and M. G. Raizen, Nat. Phys. **7**, 527 (2011).
[22] J. Gieseler, B. Deutsch, R. Quidant, and L. Novotny, Phys. Rev. Lett. **109**, 103603 (2012).
[23] N. Kiesel, F. Blaser, U. Delic, D. Grass, R. Kaltenbaek, and M. Aspelmeyer, Proc. Natl. Acad. Sci. USA **110**, 14180 (2013).
[24] D. C. Moore, A. D. Rider, and G. Gratta, Phys. Rev. Lett. **113**, 251801 (2014).
[25] J. Millen, P. Z. G. Fonseca, T. Mavrogordatos, T. S. Monteiro, and P. F. Barker, Phys. Rev. Lett. **114**, 123602 (2015).
[26] J. A. Lock and G. Gouesbet, J. Quant. Spectrosc. Radiat. Transfer **110**, 800 (2009).
[27] Y. Roichman, B. Sun, A. Stolarski, and D. G. Grier, Phys. Rev. Lett. **101**, 128301 (2008).
[28] P. Wu, R. Huang, C. Tischer, A. Jonas, and E.-L. Florin, Phys. Rev. Lett. **103**, 108101 (2009).
[29] J. Millen, T. Deesuwan, P. Barker, and J. Anders, Nat. Nanotechnol. **9**, 425 (2014).
[30] R. Kitamura, L. Pilon, and M. Jonasz, Appl. Opt. **46**, 8118 (2007).
[31] N. A. Fuchs, *The Mechanics of Aerosols* (Pergamon Press Ltd, Oxford, 1964), Chap. II; G. Hettner, Z. Phys. **37**, 179 (1926).
[32] S. A. Beresnev, V. G. Chernyak, and G. A. Fomyagin, J. Fluid Mech. **219**, 405 (1990).
[33] J. Stutz, Master's thesis, University of Nevada, 2014.
[34] B. Rodenburg, L. P. Neukirch, A. N. Vamivakas, and M. Bhattacharya, arXiv:1503.05233.